Bioconjugate Chemistry

Article

pubs.acs.org/bc

Aggregate Enhanced Trimodal Porphyrin Shell Microbubbles for Ultrasound, Photoacoustic, and Fluorescence Imaging

Elizabeth Huynh,[†,‡] Cheng S. Jin,[†,§] Brian C. Wilson,[†,‡] and Gang Zheng*[,†,‡,§]

[†]Princess Margaret Cancer Centre and Techna Institute, University Health Network, Toronto, Ontario M5G1L7, Canada

[‡]Department of Medical Biophysics and [§]Institute of Biomaterials and Biomedical Engineering, University of Toronto, Ontario M5G1L7, Canada

ABSTRACT: Microbubbles (MBs) are currently used as ultrasound (US) contrast agents and as delivery vehicles for site-specific US-triggered drug and gene delivery. Multimodal US-based imaging methods have been applied preclinically to assess and validate the effectiveness and fate of MBs in imaging and therapy. Here we present the first intrinsically trimodal MBs by incorporating a dense concentration of porphyrin molecules within a MB shell, enabled by the use of a single porphyrin-lipid component. These MBs possess US, photoacoustic, and fluorescence properties that are demonstrated in solution and in a mouse tumor xenograft model. They also have potential to be extended to other imaging modalities such as magnetic resonance imaging and nuclear imaging.

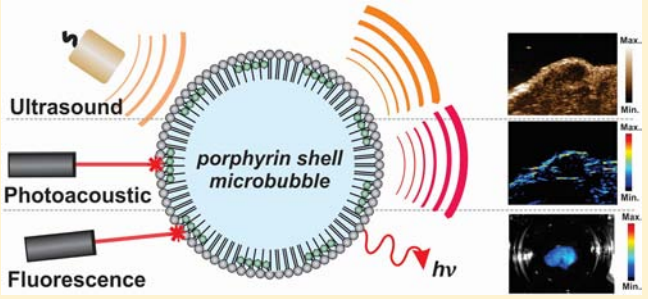

INTRODUCTION

Contrast-enhanced ultrasound (US) imaging has been implemented in routine clinical practice for diagnostic imaging of a number of organs and pathologies, including the assessment of malignant liver lesions[1] and echocardiography.[2] These agents are typically gas-filled microbubbles (MBs) stabilized by a shell composed of lipids, polymers, or proteins. The high ultrasonic backscatter properties and ability to compress and expand in response to acoustic waves at clinically relevant frequencies make them excellent contrast agents for imaging of functional and molecular vascular properties.[3]

There has been growing interest in the field of multimodal imaging utilizing MBs, which have been suggested for different potential applications:[3] for example, radiolabeled MBs have been developed for nuclear imaging to assess biodistributions,[4,5] while fluorescent MBs have been used to validate binding to biological targets.[6,7] The generation of multimodality MBs typically involves encapsulation, adsorption, and/or tethering to the MB shell of imaging reporter moieties such as nanoparticles, radiotracers, or small molecules. The amount of reporter that can be carried by a MB depends on shell properties such as thickness and charge. As a result of their thin shell (~3 nm), lipid MBs provide the best ultrasound contrast due to their ability to easily compress and expand compared to thick-shelled polymer or protein MBs (~50−500 nm), but have the lowest loading capacity.[3] Furthermore, synthesizing multicomponent multifunctional MBs is challenging due to the multistep process, which can lead to uncontrolled heterogeneity of MB properties and complicated toxicity studies in which the multiple components must each be tracked.[8]

To overcome these limitations, we previously demonstrated MBs with up to 15 molar % porphyrin−lipid content.[9] Porphyrin−lipid conjugates behave similarly to regular phospholipids, but with the added unique characteristic of very strong interactions with light.[10−15] These porphyrin−lipid shell MBs, termed "porshe MBs", have both ultrasound and photoacoustic (PA) properties, rendering them as dual-modality contrast agents. The gaseous core generated the acoustic contrast, while the dense packing of porphyrins within the microbubble shell gives very high optical absorption that generates strong PA signals. In addition, the unique intrinsic metal chelation characteristics of porphyrins, such as pyropheophorbide-α (pyro), enables porshe MB contrast for radionuclide imaging by insertion of copper-64 into the porphyrin ring structure[16,17] or magnetic resonance imaging (MRI) by insertion of manganese,[18] without requiring additional nanoparticles, chelators, or small molecules.

In formulating these porshe MBs, we observed a distinct shift in the Q-band absorbance from that of the monomeric porphyrin, a characteristic of ordered aggregation. Although ordered aggregation can result in the generation of fluorescence,[19] we did not observe this in practice due to the relatively low porphyrin content. Here we report a significantly improved porshe MB construct in which the porphyrin content was increased to 50 molar % porphyrin−lipid. We also observed ordered aggregation, and fluorescence generation was also detectable. Hence, these porshe MBs are the first intrinsically trimodal contrast agent for US, PA, and

Received: February 19, 2014
Revised: March 9, 2014
Published: March 12, 2014

   dx.doi.org/10.1021/bc5000725 | *Bioconjugate Chem.* 2014, 25, 796−801

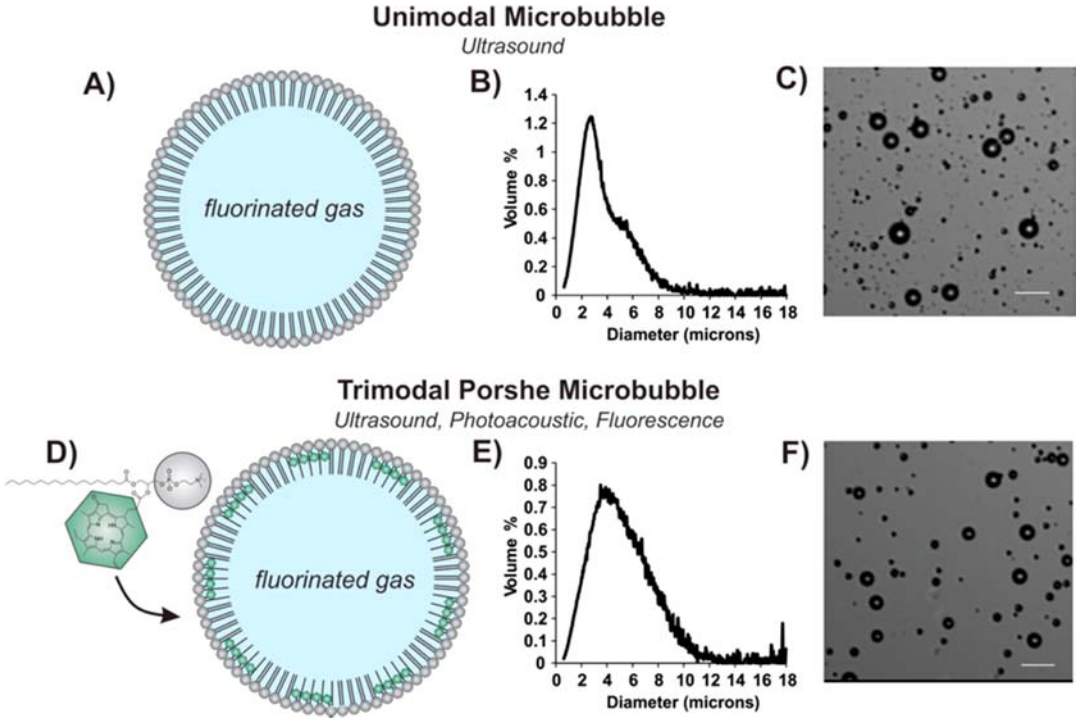

Figure 1. Unimodal and trimodal porshe microbubbles. Schematic representations of (A) MBs formed from regular phospholipids (unimodal MBs) and (D) MBs including porphyrin-phospholipids (pyro-lipid). Corresponding size distributions (B, E) and light microscopy images (C, F). Scale bar 10 μm.

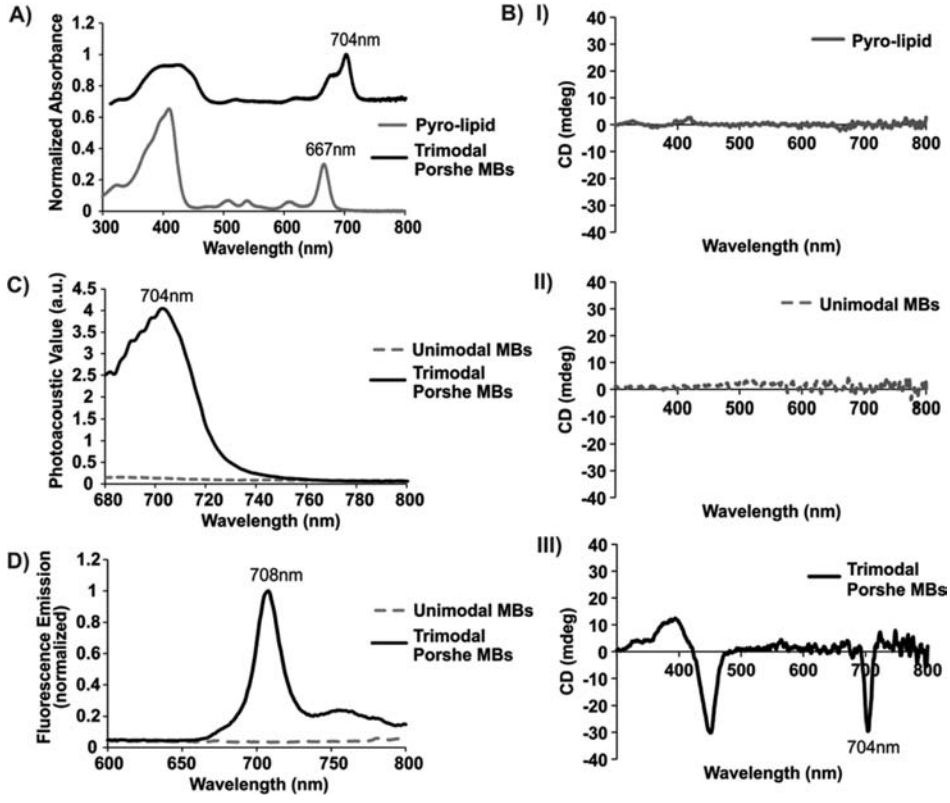

Figure 2. (A) Absorbance spectra of trimodal porshe MBs in phosphate buffered saline (PBS) and monomeric pyro-lipid in 1% Triton-X (detergent). The difference in the background is due to light scattering of the MBs. (B) Circular dichroism spectra of pyro-lipid in detergent (I), unimodal MBs (II), and trimodal porshe MBs (III) in PBS. (C) PA spectra of unimodal and trimodal porshe MBs in PBS. (D) Corresponding fluorescence emission spectra under 410 nm excitation.

dx.doi.org/10.1021/bc5000725 | *Bioconjugate Chem.* 2014, 25, 796−801

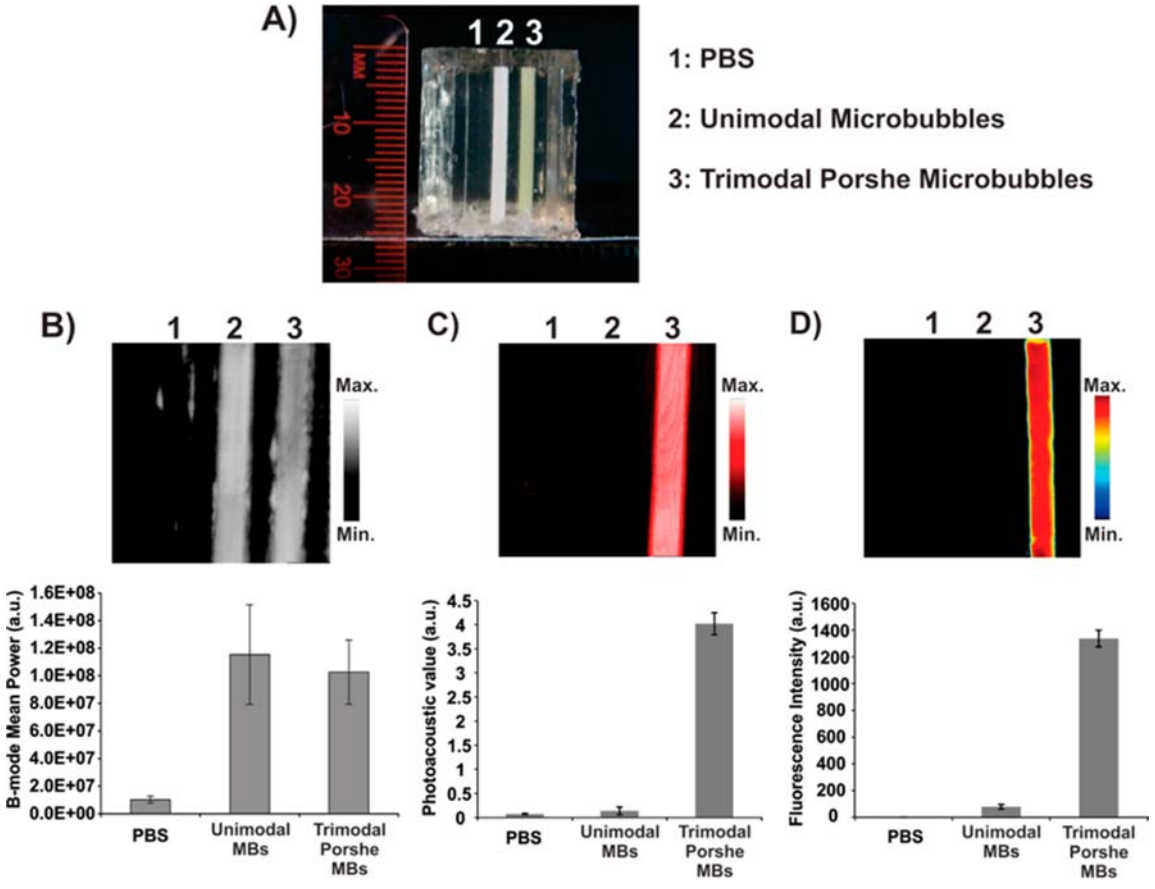

Figure 3. Trimodal imaging in solution. White light image (A) of the gelatin holder containing three samples: (1) PBS only, (2) unimodal porshe MBs, and (3) trimodal porshe MBs. The MBs were matched in concentration (10^9 MBs/mL). (B) US (21 MHz), (C) PA (704 nm, 21 MHz), and (D) fluorescence (435−480 nm excitation, >515 nm detection) images and corresponding signal intensities (mean ±1 SD from 3 measurements).

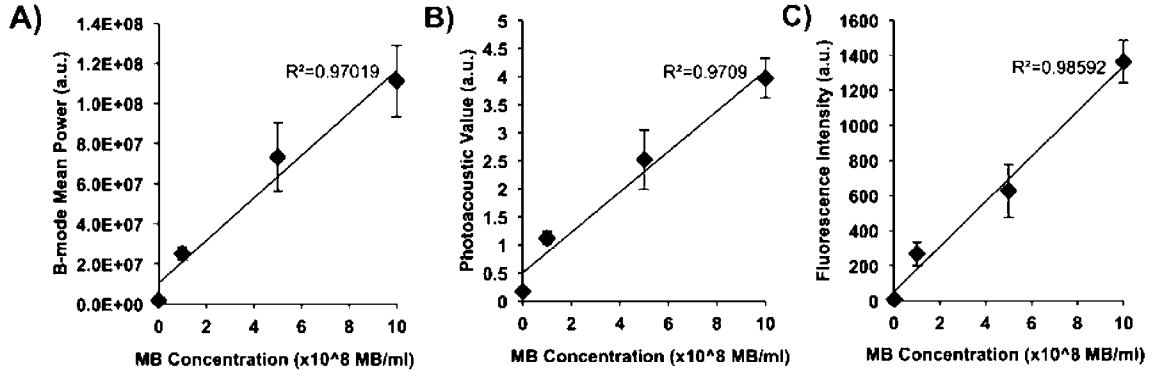

Figure 4. Concentration dependence of the US (A), PA (B), and fluorescence (C) signals from trimodal porshe MBs in the gelatin phantom. Means ±1 SD from 3 measurements. The linear regression lines are shown.

fluorescence imaging, which expands their potential clinical utility and applications.

■ RESULTS AND DISCUSSION

Unimodal and trimodal porshe MBs were formed by lipid film rehydration and mechanical agitation. Unimodal MBs were composed of 90 molar % 1,2-distearoyl-*sn*-glycero-3-phosphocholine (DSPC) and 10 molar % 1,2-distearoyl-*sn*-glycero-3-phosphoethanolamine-*N*-[methoxy(polyethylene glycol)-2000] (DSPE-mPEG2000) encapsulating perfluoropropane gas (Figure 1a). Trimodal porshe MBs were prepared in a similar manner but with the substitution of 50 molar % regular phospholipid (DSPC) by porphyrin−lipid (pyro-lipid) (Figure 1d). The resulting MBs were separated from submicrometer particles by differential centrifugation,[20] giving a size distribution between 2 and 6 μm at a concentration of 2×10^9 MBs/mL (Figure 1b,c,e,f). The absorbance spectrum of the MBs in phosphate buffered saline (PBS) displayed a Q-band peak at 704 nm, which is 37 nm red-shifted from the pyro monomeric peak wavelength (Figure 2a).

This red-shifted peak is an indication of ordered aggregation of the porphyrins within the MB shell, which was further confirmed by the presence of circularly polarized light in the circular dichroism spectrum of only the trimodal porshe MBs at

dx.doi.org/10.1021/bc5000725 | *Bioconjugate Chem.* 2014, 25, 796−801

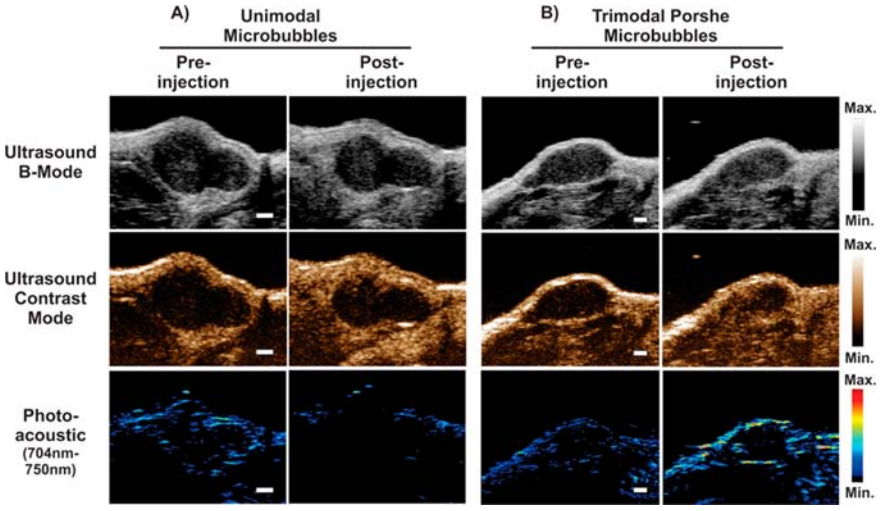

Figure 5. *In vivo* imaging of MBs in a KB tumor xenograft at 10−30 s post intravenous injection of 280 μL of MB-PBS solution at a concentration of 2×10^9 MBs/mL. The US B-mode images (top) show the soft tissue contrast of the tumor. The US contrast mode images (middle) and the photoacoustic images (bottom) show the infusion of MBs by an increase in signal. Scale bar 1 mm.

704 nm (Figure 2b). The optical absorption spectra dictates the photoacoustic spectrum, since PA imaging is based on the absorption of light and resulting transient thermoelastic expansion that generates acoustic waves.[21] The measured PA spectrum corresponded well with the absorption spectrum, with a peak PA signal at 704 nm. By comparison, since regular phospholipids are weakly light absorbing in the visible/near-infrared range, unimodal MBs did not show any distinct peaks in the PA spectrum (Figure 2c). Ordered aggregation is known to result in the generation of fluorescence,[19] which was exhibited by porshe MBs, which had a Stokes shift of 4 nm with the fluorescence emission peak at 708 nm (Figure 2d).

To further investigate the imaging properties of the trimodal porshe MBs, a US transparent gelatin holder was formed with three empty cavities which were used to immobilize the MB solutions (Figure 3a). Unimodal and trimodal porshe MBs in PBS were inserted into the cavities in the gelatin holder at equal MB concentrations (10^9 MBs/mL) and imaged using US, PA, and fluorescence (Figures 3b,c,d; top). Both MBs generated nearly equal US signals, but the trimodal MBs generated approximately 40 times higher PA signal and 17 times higher fluorescence signal (Figures 3b,c,d; bottom). The trimodal MBs exhibited concentration-dependent US, PA, and fluorescence properties, increasing linearly with concentration (Figure 4), confirming their potential as a trimodal imaging agent.

In order to demonstrate the applicability of the MBs as trimodal contrast agents, mice bearing KB tumor xenografts were administered either unimodal MBs or trimodal porshe MBs via tail vein injection and imaged *in vivo* sequentially by US, PA, and fluorescence. B-mode US images were captured to exhibit the soft tissue contrast from the tumor (Figure 5, top). Increase in the US contrast signal was observed for both unimodal and trimodal MBs; however, the MBs did not distribute homogenously within the tumor, potentially indicating the presence of a necrotic core within the tumor (Figure 5, middle). PA images were captured pre- and postinjection of both MB formulations, and only the trimodal porshe MBs showed detectable increase in PA signal after injection (Figure 5, bottom). Furthermore, the porphyrin (pyro) naturally accumulates in tumor tissue 2−3-fold higher than in normal tissue[22] so that *ex vivo* fluorescence imaging of the resected tumors confirmed the tumor uptake of the trimodal porshe MBs and generation of significant fluorescence signal compared with the unimodal MBs (Figure 6). This

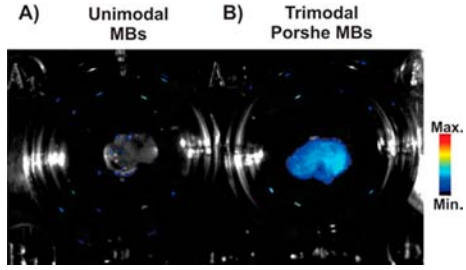

Figure 6. *Ex vivo* fluorescence imaging of KB tumor at 4 h after i.v. administration of unimodal (A) or trimodal porshe MBs (B). 435−480 nm excitation, >515 nm detection, overlaid with gray-scale white light images.

fluorescence property of trimodal porshe MBs could be used as an *ex vivo* validation tool to confirm tumor binding and uptake and biodistribution of porshe MB fragments postinjection or potentially also *in vivo*, by external, endoscopic, or intra-operative imaging, depending on the tumor location and clinical application. These images collectively confirm the ability of trimodal porshe MBs to function as a trimodality contrast agent.

In addition to the ability to behave as a trimodal contrast agent for US, PA, and fluorescence imaging, the generation of microbubbles with optical properties presents a unique opportunity to apply ultrasound-specific properties to an optical-contrast agent and vice versa. For example, MBs have been investigated for drug delivery or for crossing the blood-brain barrier through spatially localized ultrasonic bursting of the bubbles.[23−25] This does not allow real-time tracking of the resulting fragmented MB, since the acoustic signal is lost upon bursting. However, with the intrinsic optical properties imparted by the porphyrin−lipid in the trimodal porshe MBs, real-time tracking may be possible using photoacoustic imaging, with validation using fluorescence. A converse example would be the use of acoustic contrast to track the MBs volumetrically and noninvasively so that the optimum time for fluorescence

dx.doi.org/10.1021/bc5000725 | *Bioconjugate Chem.* 2014, 25, 796−801

imaging could be determined such as in surgical guidance. These options are under investigation. In addition to the trimodal properties of these porshe MBs, the increase in porphyrin content opens a window of opportunity for combined ultrasound and optical imaging with, for example, MRI using manganese-conjugated porphyrins.

CONCLUSIONS

We have generated porshe MBs in which the porphyrin content is increased by 3-fold from 15 to 50 molar %, resulting in fluorescence produced from ordered aggregation and high optical absorption, thereby generating an intrinsically trimodal agent for ultrasound, photoacoustic, and fluorescence imaging based on a single-component porphyrin−lipid structure. Importantly, this multimodal capability is achieved without the complexity and potential errors of combining multiple separate imaging components. The increased porphyrin content has been shown to enable photoacoustic and fluorescence imaging in addition to the previously reported ultrasound properties of regular phospholipid microbubbles,[26] expanding the multimodality imaging applications.

EXPERIMENTAL PROCEDURES

Porshe Microbubble Fabrication and Characterization. Lipid films were prepared in 12 mm × 35 mm clear glass threaded vials (Fisher Scientific) by combining 0.5 mg of 50 molar % porphyrin−lipid (pyropheophorbide-lipid; as previously described[26] except that 1-stearoyl-2-hydroxy-sn-glycero-3-phosphocholine was used as the starting lipid instead of 1-palmitoyl-2hydroxy-sn-glyer-3-phosphocholine) together with 40 molar % 1,2-distearoyl-sn-glycero-3-phosphocholine (DSPC) and 10 molar % 1,2-distearoyl-sn-glycero-3-phosphoethanolamine-N-[methoxy(polyethylene glycol)-2000] (DSPE-mPEG2000) in chloroform, and dried by nitrogen gas and vacuum. Lipid films were then rehydrated with 1 mL of 10 vol % propylene glycol, 10 vol % glycerol, and 80 vol % phosphate buffered saline. Samples were then briefly heated and sonicated to disperse the lipid film, topped with perfluoropropane gas (C_3F_8, PFP, Fluoromed L.P) and then mechanically agitated using a VialMix shaker for 45 s. After activation, vials containing the agent were passively cooled to room temperature over 15 min before use and then used within 3 h. For use, the microbubbles were gently mixed by hand for 10 s and then decanted for 2 min before extracting a sample from the bottom of the vial. The resulting MBs were separated from submicrometer particles by differential centrifugation[20] at 50 *g* for 8 min. The resulting microbubble cake was resuspended with 10 vol % propylene glycol, 10 vol % glycerol, and 80 vol % phosphate buffered saline (PBS).

The size distribution and concentration of each formulation was measured with a Coulter Counter Multisizer Z3 (Beckman Coulter Inc.). For this, 20 μL of microbubbles were extracted and added to 10 mL of Isoton-II electrolyte solution (Beckman Coulter Inc.) to obtain a microbubble count in the range of 100,000−300,000. A background count of buffer was taken immediately prior to this measurement and subtracted. Dilution was accounted for in calculating the microbubble concentration. The number and size distribution were measured using a 30 μm aperture which detected microbubbles with diameters in the range 0.76−18 μm. Three samples were measured and averaged for each microbubble formulation.

Absorption spectra were determined by UV spectroscopy (CARY 50 UV/vis S3 Spectrophotometer, Varian Inc.) in PBS for the porshe MBs spectrum and in 1% Triton X-100 for the pyro-lipid spectrum. Circular dichroism spectra were determined in PBS for unimodal MBs and trimodal porshe MBs and in 1% Triton X-100 for pyro-lipid using a J-815 Circular Dichroism Spectrometer (JASCO Inc.). Fluorescence spectra were determined in PBS using a Flouromax fluorometer (Horiba Jobin Yvon) with an excitation wavelength of 410 nm and a 5 nm slit width, collecting the fluorescence emission from 600 to 800 nm using a 5 nm slit width.

Trimodal Imaging in Solution. PBS, unimodal, and trimodal porshe MB solutions were placed in an US-transparent holder made of 20% gelatin at a concentration of 120 μL of 10^9 MBs/mL. Ultrasound and photoacoustic imaging were conducted using a commercial photoacoustic imaging system (Vevo LAZR: FUJIFILM VisualSonics, Inc.), operating with a 21 MHz transducer in both ultrasound and photoacoustic modes. Photoacoustic spectra were obtained from 680 to 800 nm. Fluorescence images were obtained using a whole-body small animal imager (CRi Maestro: Caliper Life Science Inc.) under blue-light excitation (435−480 nm), 515 nm long pass detection, and an integration time of 600 ms.

In Vivo Trimodal Imaging. Animal experiments were performed in compliance with institutional animal care approval (University Health Network, Toronto) using nude mice bearing KB tumor xenografts. The model was generated by subcutaneous inoculation of 2×10^6 KB cells in PBS in the flank of adult female Nu/nu mice. Imaging was performed when the tumors achieved a surface diameter of 4−5 mm (~10 days). For the imaging, the mice were anesthetized with 2% (v/v) isoflurane inhalation and 280 μL of 2×10^9 MB/mL unimodal MBs or trimodal porshe MBs was injected via the tail vein. Acoustic coupling gel was applied over the tumor and the mice were then imaged over the tumor region in both ultrasound and photoacoustic mode. Final photoacoustic images were obtained by subtracting images acquired at 704 nm from those acquired at 750 nm where the porshe MBs do not absorb significantly in order to remove background signal as a result of blood. At 4 h after microbubble injection the mice were sacrificed by cervical dislocation under general anesthetic and the tumors were resected, placed in PBS, and imaged in fluorescence mode (4000 ms integration time).

AUTHOR INFORMATION

Corresponding Author

*E-mail: gzheng@uhnresearch.ca.

Notes

The authors declare no competing financial interest.

ACKNOWLEDGMENTS

This work was supported by an International Collaborative R&D Project of the Ministry of Knowledge Economy, South Korea, with additional personnel support from the Natural Sciences and Engineering Research Council of Canada, the Canadian Institutes of Health Research and the Ontario Institute for Cancer Research and infrastructure support from the Canada Foundation for Innovation and the Princess Margaret Cancer Centre Foundation.

REFERENCES

(1) Claudon, M., Cosgrove, D., Albrecht, T., Bolondi, L., Bosio, M., Calliada, F., Correas, J. M., Darge, K., Dietrich, C., D'Onofrio, M., Evans, D. H., Filice, C., Greiner, L., Jager, K., Jong, N., Leen, E., Lencioni, R., Lindsell, D., Martegani, A., Meairs, S., Nolsoe, C., Piscaglia, F., Ricci, P., Seidel, G., Skjoldbye, B., Solbiati, L., Thorelius, L., Tranquart, F., Weskott, H. P., and Whittingham, T. (2008) Guidelines and good clinical practice recommendations for contrast enhanced ultrasound (CEUS) - update 2008. *Ultraschall. Med. 29*, 28−44.

(2) Mulvagh, S. L., Rakowski, H., Vannan, M. A., Abdelmoneim, S. S., Becher, H., Bierig, S. M., Burns, P. N., Castello, R., Coon, P. D., Hagen, M. E., Jollis, J. G., Kimball, T. R., Kitzman, D. W., Kronzon, I., Labovitz, A. J., Lang, R. M., Mathew, J., Moir, W. S., Nagueh, S. F., Pearlman, A. S., Perez, J. E., Porter, T. R., Rosenbloom, J., Strachan, G. M., Thanigaraj, S., Wei, K., Woo, A., Yu, E. H., and Zoghbi, W. A. (2008) American Society of, E., American Society of Echocardiography consensus statement on the clinical applications of ultrasonic contrast agents in echocardiography. *J. Am. Soc. Echocardiogr. 21*, 1179−201.

(3) Kiessling, F., Fokong, S., Bzyl, J., Lederle, W., Palmowski, M., and Lammers, T. (2013) Recent advances in molecular, multimodal and theranostic ultrasound imaging. *Adv. Drug Delivery Rev.*, DOI: 10.1016/j.addr.2013.11.013.

(4) Tartis, M. S., Kruse, D. E., Zheng, H., Zhang, H., Kheirolomoom, A., Marik, J., and Ferrara, K. W. (2008) Dynamic microPET imaging of ultrasound contrast agents and lipid delivery. *J. Controlled Release 131*, 160−6.

(5) Lazarova, N., Causey, P. W., Lemon, J. A., Czorny, S. K., Forbes, J. R., Zlitni, A., Genady, A., Foster, F. S., and Valliant, J. F. (2011) The synthesis, magnetic purification and evaluation of 99mTc-labeled microbubbles. *Nucl. Med. Biol. 38*, 1111−8.

(6) Lindner, J. R., Coggins, M. P., Kaul, S., Klibanov, A. L., Brandenburger, G. H., and Ley, K. (2000) Microbubble persistence in the microcirculation during ischemia/reperfusion and inflammation is caused by integrin- and complement-mediated adherence to activated leukocytes. *Circulation 101*, 668−75.

(7) Lum, A. F., Borden, M. A., Dayton, P. A., Kruse, D. E., Simon, S. I., and Ferrara, K. W. (2006) Ultrasound radiation force enables targeted deposition of model drug carriers loaded on microbubbles. *J. Controlled Release 111*, 128−34.

(8) Huynh, E., and Zheng, G. (2013) Engineering multifunctional nanoparticles: all-in-one versus one-for-all. *Wiley Interdiscip. Rev.: Nanomed. Nanobiotechnol. 5*, 250−65.

(9) Huynh, E., Lovell, J. F., Helfield, B. L., Jeon, M., Kim, C., Goertz, D. E., Wilson, B. C., and Zheng, G. (2012) Porphyrin shell microbubbles with intrinsic ultrasound and photoacoustic properties. *J. Am. Chem. Soc. 134*, 16464−7.

(10) Lovell, J. F., Jin, C. S., Huynh, E., Jin, H., Kim, C., Rubinstein, J. L., Chan, W. C., Cao, W., Wang, L. V., and Zheng, G. (2011) Porphysome nanovesicles generated by porphyrin bilayers for use as multimodal biophotonic contrast agents. *Nat. Mater. 10*, 324−32.

(11) Lovell, J. F., Jin, C. S., Huynh, E., MacDonald, T. D., Cao, W., and Zheng, G. (2012) Enzymatic regioselection for the synthesis and biodegradation of porphysome nanovesicles. *Angew. Chem., Int. Ed. 51*, 2429−33.

(12) Jin, C. S., Lovell, J. F., Chen, J., and Zheng, G. (2013) Ablation of hypoxic tumors with dose-equivalent photothermal, but not photodynamic, therapy using a nanostructured porphyrin assembly. *ACS Nano 7*, 2541−50.

(13) Ng, K. K., Lovell, J. F., Vedadi, A., Hajian, T., and Zheng, G. (2013) Self-assembled porphyrin nanodiscs with structure-dependent activation for phototherapy and photodiagnostic applications. *ACS Nano 7*, 3484−90.

(14) Tam, N. C., McVeigh, P. Z., MacDonald, T. D., Farhadi, A., Wilson, B. C., and Zheng, G. (2012) Porphyrin-lipid stabilized gold nanoparticles for surface enhanced Raman scattering based imaging. *Bioconjugate Chem. 23*, 1726−30.

(15) Jin, C. S., Cui, L., Wang, F., Chen, J., and Zheng, G. (2014) Targeting-triggered porphysome nanostructure disruption for activatable photodynamic therapy. *Adv. Healthcare Mater.*, 1−10.

(16) Liu, T. W., MacDonald, T. D., Shi, J., Wilson, B. C., and Zheng, G. (2012) Intrinsically copper-64-labeled organic nanoparticles as radiotracers. *Angew. Chem., Int. Ed. 51*, 13128−31.

(17) Liu, T. W., Macdonald, T. D., Jin, C. S., Gold, J. M., Bristow, R. G., Wilson, B. C., and Zheng, G. (2013) Inherently multimodal nanoparticle-driven tracking and real-time delineation of orthotopic prostate tumors and micrometastases. *ACS Nano 7*, 4221−32.

(18) Chen, C. W., Cohen, J. S., Myers, C. E., and Sohn, M. (1984) Paramagnetic metalloporphyrins as potential contrast agents in NMR imaging. *FEBS Lett. 168*, 70−4.

(19) Wurthner, F., Kaiser, T. E., and Saha-Moller, C. R. (2011) J-aggregates: from serendipitous discovery to supramolecular engineering of functional dye materials. *Angew. Chem., Int. Ed. 50*, 3376−410.

(20) Feshitan, J. A., Chen, C. C., Kwan, J. J., and Borden, M. A. (2009) Microbubble size isolation by differential centrifugation. *J. Colloid Interface Sci. 329*, 316−24.

(21) Wang, L. V., and Hu, S. (2012) Photoacoustic tomography: in vivo imaging from organelles to organs. *Science 335*, 1458−62.

(22) Berg, K., Selbo, P. K., Weyergang, A., Dietze, A., Prasmickaite, L., Bonsted, A., Engesaeter, B. O., Angell-Petersen, E., Warloe, T., Frandsen, N., and Hogset, A. (2005) Porphyrin-related photosensitizers for cancer imaging and therapeutic applications. *J. Microsc. 218*, 133−47.

(23) Hernot, S., and Klibanov, A. L. (2008) Microbubbles in ultrasound-triggered drug and gene delivery. *Adv. Drug Delivery Rev. 60*, 1153−66.

(24) Ferrara, K., Pollard, R., and Borden, M. (2007) Ultrasound microbubble contrast agents: fundamentals and application to gene and drug delivery. *Annu. Rev. Biomed. Eng. 9*, 415−47.

(25) Klibanov, A. L. (2006) Microbubble contrast agents: targeted ultrasound imaging and ultrasound-assisted drug-delivery applications. *Invest. Radiol. 41*, 354−62.

(26) Aref'ev, I. M. (1986) Current status and major trends in the development of medical laser technology. *Med. Tekh. 4*, 40−5.